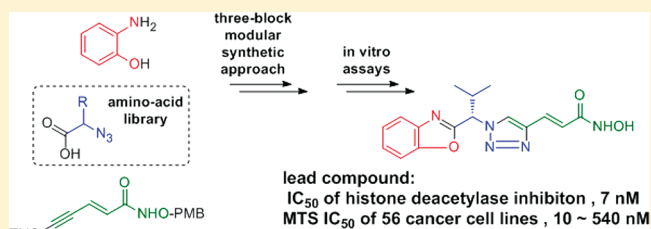


Discovery and Extensive *in Vitro* Evaluations of NK-HDAC-1: A Chiral Histone Deacetylase Inhibitor as a Promising LeadJingli Hou,<sup>‡,||</sup> Zhonghua Li,<sup>‡,||</sup> Qinghong Fang,<sup>‡</sup> Congran Feng,<sup>‡</sup> Hanwen Zhang,<sup>‡</sup> Weikang Guo,<sup>‡</sup> Huihui Wang,<sup>‡</sup> Guoxian Gu,<sup>‡</sup> Yinping Tian,<sup>‡</sup> Pi Liu,<sup>‡</sup> Ruihua Liu,<sup>‡</sup> Jianping Lin,<sup>‡</sup> Yi-kang Shi,<sup>§</sup> Zheng Yin,<sup>†,‡</sup> Jie Shen,<sup>\*,†,‡</sup> and Peng George Wang<sup>\*,†,‡</sup><sup>†</sup>State Key Laboratory of Medicinal Chemical Biology, Nankai University, Tianjin, China<sup>‡</sup>College of Pharmacy, Nankai University, Tianjin, China<sup>§</sup>National Glycoengineering Research Center, Shandong University, 44 West Wenhua Road, Jinan, China

## S Supporting Information

**ABSTRACT:** Herein, further SAR studies of lead compound NSC746457 (Shen, J.; Woodward, R.; Kedenburg, J. P.; Liu, X. W.; Chen, M.; Fang, L. Y.; Sun, D. X.; Wang, P. G. *J. Med. Chem.* 2008, 51, 7417–7427) were performed, including the replacement of the *trans*-styryl moiety with a 2-substituted benzo-hetero aromatic ring and the introduction of a substituent onto the central methylene carbon. A promising chiral lead, *S*-(*E*)-3-(1-(1-(benzo[*d*]oxazol-2-yl)-2-methylpropyl)-1*H*-1,2,3-triazol-4-yl)-*N*-hydroxyacrylamide (**12**, NK-HDAC-1), was discovered and showed about 1 order of magnitude more potency than SAHA in both enzymatic and cellular assays. For the *in vitro* safety tests, NK-HDAC-1 was far less toxic to nontransformed cells than tumor cells and showed no significant inhibition activity against CYP-3A4. The pharmaceutical properties (LogD, solubility, liver microsomal stability (*t*<sub>1/2</sub>), plasma stability (*t*<sub>1/2</sub>), and apparent permeability) strongly suggested that NK-HDAC-1 might be superior to SAHA in bioavailability and *in vivo* half-life.



## INTRODUCTION

The reversible acetylation and deacetylation modifications of lysine residues of histones can regulate gene expression via remodeling chromatin architecture.<sup>2–8</sup> Histone acetyltransferases (HATs) can relax chromatin and epigenetically promote gene transcription. Conversely, histone deacetylases (HDACs) can condense chromatin and epigenetically prevent gene transcription. Besides histones, a large number of nonhistone client proteins of HDACs and HATs were identified, such as transcription factors, hormone receptors, chaperone protein, cytoskeletal protein, etc.<sup>9,10</sup> Accordingly, multiple antitumor mechanisms of HDACi were suggested, including alteration of gene expression, degradation of Hsp90 client proteins, increased production of reactive oxygen species, induction of cell cycle arrest, etc. To date, there are more than 10 HDACi molecules entering into clinical trials (Figure 1). SAHA and Romidepsin, the first two marketed HDACi drugs, were approved by the FDA in 2006 and 2009, respectively, for the treatment of cutaneous T-cell lymphoma (CTCL).

There are 18 HDAC isozymes encoded in the human genome, and they are divided into four classes. Class III isozymes, including Sirt1 to Sirt7, utilize NAD<sup>+</sup> as a cofactor. The other three classes (Class I, HDAC1, 2, 3, and 8; Class II, HDAC 4, 5, 6, and 9; and Class IV, HDAC 11) are Zn-dependent isozymes. Co-crystals of HDAC bound with HDACi<sup>11</sup> highlight a common molecular scaffold for Zn-

dependent HDACi: a Zn<sup>2+</sup> binding group (ZBG) positioned at the bottom of a highly conserved “tube-like” active site, a “cap” region which can interact with the rim of the HDAC active pocket, and a linker which fits in the hydrophobic “tube” (Figures 1 and 2).

In our recent works,<sup>1</sup> click chemistry was employed to afford a highly efficient combinatorial approach to constructing a library of new HDACi candidates, and a hit compound (NSC746457) was discovered which showed comparable activity to SAHA. The triazole ring was of suitable size to fit into the narrow active pocket of HDAC protein. Moreover, the triazole ring was correctly positioned to form a  $\pi$ - $\pi$  interaction with two reserved phenylalanine residues in the docking structure of NSC746457 with HDAC2 (Figure 2). This indicated that, besides the role of linker moiety, the triazole ring in our design also contributed to the binding affinity.

In this article, lead optimizations of NSC746457 were performed (Scheme 1), focusing on two aspects: (1) the introduction of a side chain at the methylene carbon atom and (2) the replacement of *trans*-styryl moiety with a 2-substituted benzo-hetero ring. The methylene carbon atom is at the joint position between the cap region and the linker moiety of NSC746457, and in the computational complex structure, this

Received: November 7, 2011

Published: March 21, 2012

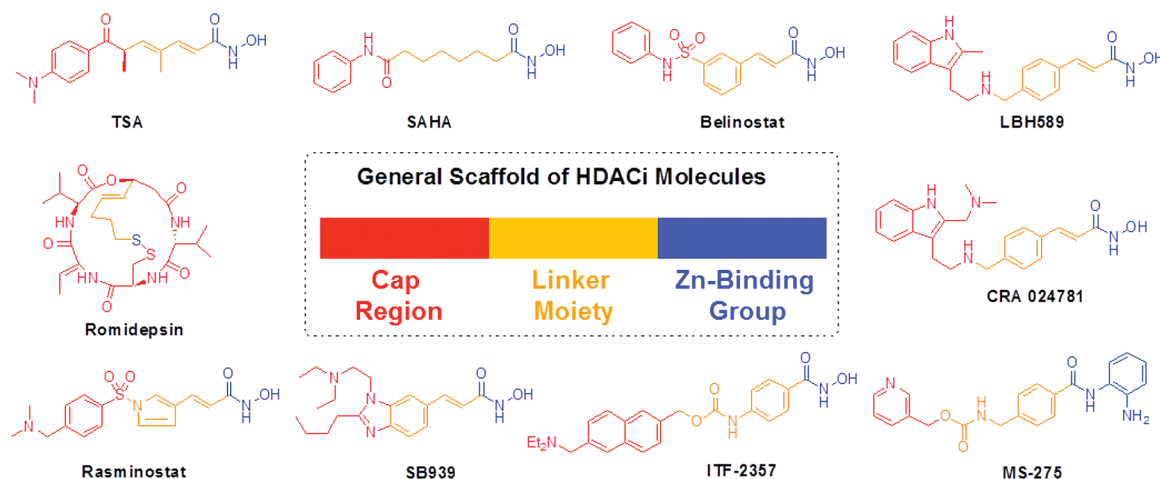


Figure 1. Structures of TSA and some HDACi molecules in clinical trials or clinical use.

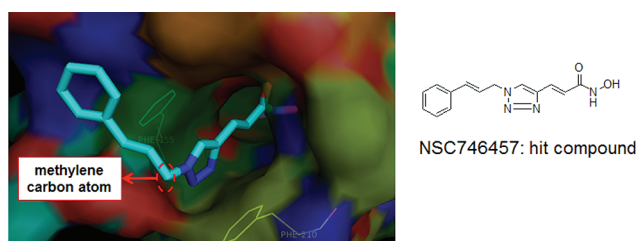
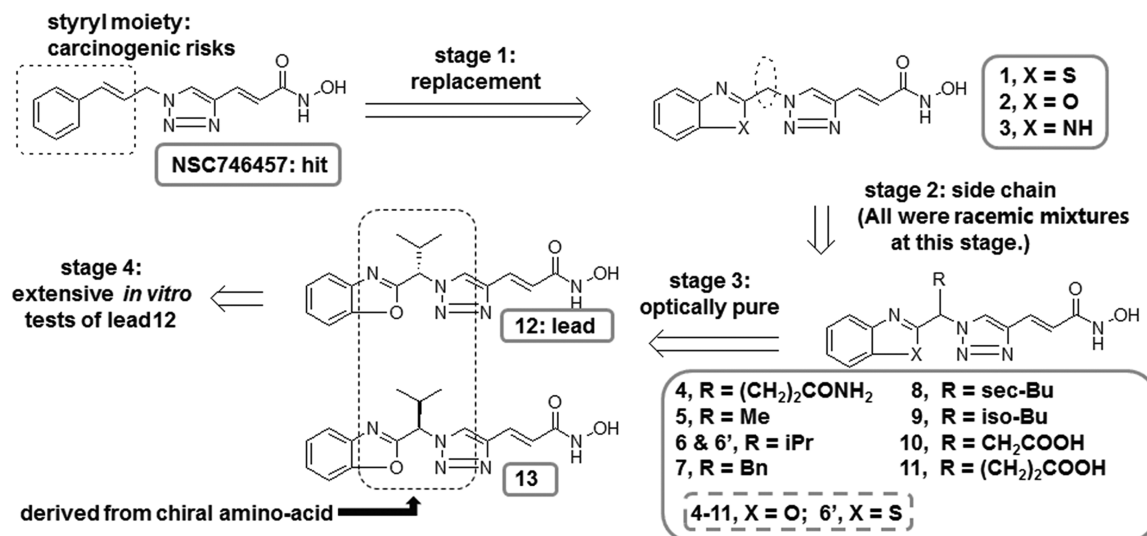


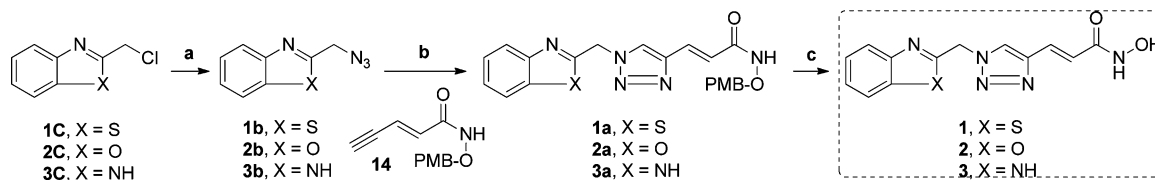
Figure 2. Docking of NSC746457 (our hit compound) into the active pocket of human HDAC2 protein.

methylene carbon atom is positioned at the open rim of the HDAC active pocket, surrounding which are several shallow grooves (Figure 2). Inspired by previous HDACi lead optimization study results,<sup>12–15</sup> we envisioned that introduction of a side chain at the methylene carbon would enhance the HDACi/HDAC binding affinity: (a) This side chain might be in contact with some shallow groove on the surface of the rim and therefore contribute to the binding affinity. (b) This side chain would restrict the free rotation of the two single bonds which flanked the newly generated chiral center. Such an

intrinsic restriction might direct the cap region of the HDACi molecule to properly be in contact with some surface groove of HDAC. There are four reasons for us to attempt the replacement of the *trans*-styryl moiety with a 2-substituted benzo-hetero ring: (1) *trans*-styryl can be considered as a bioisoster of the 2-substituted-hetero aromatic ring, and they share a similar structural scaffold; therefore, such a replacement would maintain the HDAC inhibition potency of the hit compound. (2) The possible epoxide metabolite of the styryl moiety could be a potential carcinogenic alkylation reagent<sup>16</sup> and such a replacement would avoid this toxicity concern for drug development. (3) The newly introduced side chain at the methylene carbon generates a chiral center which can be conveniently derived from chiral amino acid reactants if the *trans*-styryl moiety was replaced with a 2-substituted benzo-hetero ring. (4) Some benzo-hetero rings, such as indole and benzofuran, were successfully employed in the cap regions of some HDACi molecules in clinical trials (Figure 1). Taken together, the lead optimization studies herein were planned to proceed in four stages (Scheme 1), which are thoroughly discussed in the following sections.

#### Scheme 1. Flow Chart of Work Plan in This Article



Scheme 2. Syntheses of Target Compounds in Stage 1: 1–3<sup>a</sup>

<sup>a</sup>Reagents and conditions: (a) NaN<sub>3</sub>, DMSO, room temperature; (b) CuSO<sub>4</sub>, sodium ascorbate, rt; (c) TFA, triisopropylsilane, DCM, rt.

Table 1. *In Vitro* Efficacy Assays of Compounds in Stage 1.<sup>a</sup>

	IC <sub>50</sub> (nM) <sup>a</sup> HDACs	GI <sub>50</sub> (μM) <sup>a</sup>						
		A549 <sup>b</sup>	HepG2 <sup>b</sup>	KS62 <sup>c</sup>	SW-620 <sup>c</sup>	Colo-205 <sup>c</sup>	OVCR-3 <sup>c</sup>	PC-3 <sup>c</sup>
SAHA	67	3.1	3.5	0.50	0.63	4.0	2.0	1.6
NSC746457	104	1.9	3.2	0.55	0.48	1.1	1.1	1.3
1	41	2.1	8.8	2.6	1.5	1.5	3.6	2.9
2	105	4.7	6.1	0.72	1.2	1.1	1.9	1.6
3	178	>20	>20	ND <sup>d</sup>	ND <sup>d</sup>	ND <sup>d</sup>	ND <sup>d</sup>	ND <sup>d</sup>

<sup>a</sup>Mean of three independent triplicate experiments. <sup>b</sup>MTT data from our lab. <sup>c</sup>Selected MTS data from the program of NCI-60-human-tumor-cell-line-anticancer-drug-screen. <sup>d</sup>ND, not determined.

## RESULT AND DISCUSSION

**Stage 1: Replacement of *trans*-Styryl with a 2-Substituted Benzo-Hetero Aromatic Ring.** In this stage, the *trans*-styryl moiety was replaced with a 2-substituted benzoxazole ring, benzothiazole ring, or benzimidazole ring, resulting in three newly designed HDACi molecules 1–3. These three compounds were prepared from 2-chloromethyl substituted benzo-hetero compounds 1c–3c, which were obtained from the known procedures.<sup>17–19</sup> Compounds 1c–3c were then converted to the azido derivatives 1b–3b via nucleophilic substitution by using sodium azide solution in DMSO. Cu(I)-mediated Huisgen cycloaddition reactions of the known alkyne compound 14<sup>1</sup> were carried out with each of the azido derivatives 1b–3b to afford the click products 1a–3a. Finally, the PMB protecting group was removed by TFA (Scheme 2) to provide the target compounds 1–3. In HDAC inhibition assays (Table 1), benzothiazole derivative 1 (IC<sub>50</sub> = 41 nM) was approximately two times more potent than NSC746457 (IC<sub>50</sub> = 104 nM); benzoxazole derivative 2 (IC<sub>50</sub> = 105 nM) was comparable to NSC746457; benzimidazole derivative 3, (IC<sub>50</sub> = 178 nM) was approximately two times less potent than NSC746457. DFT calculations using Schrodinger Jaguar 7.8<sup>20</sup> revealed that compound 3 could form an intramolecular hydrogen bond to partially freeze the dominant conformation, which, however, was not like the preferred conformation of the hit compound in the docking structure (Figures 2 and 3). Such a conformation restriction was not observed in the DFT calculation for compound 2. In cell viability assays, the weak potency of compound 3 was also observed; however, compound 2 was slightly more potent than compound 1, showing results inconsistent to the HDAC

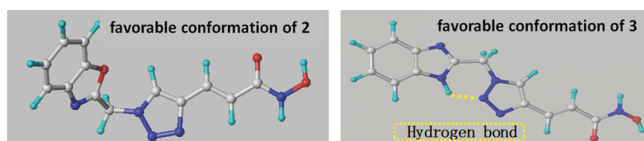
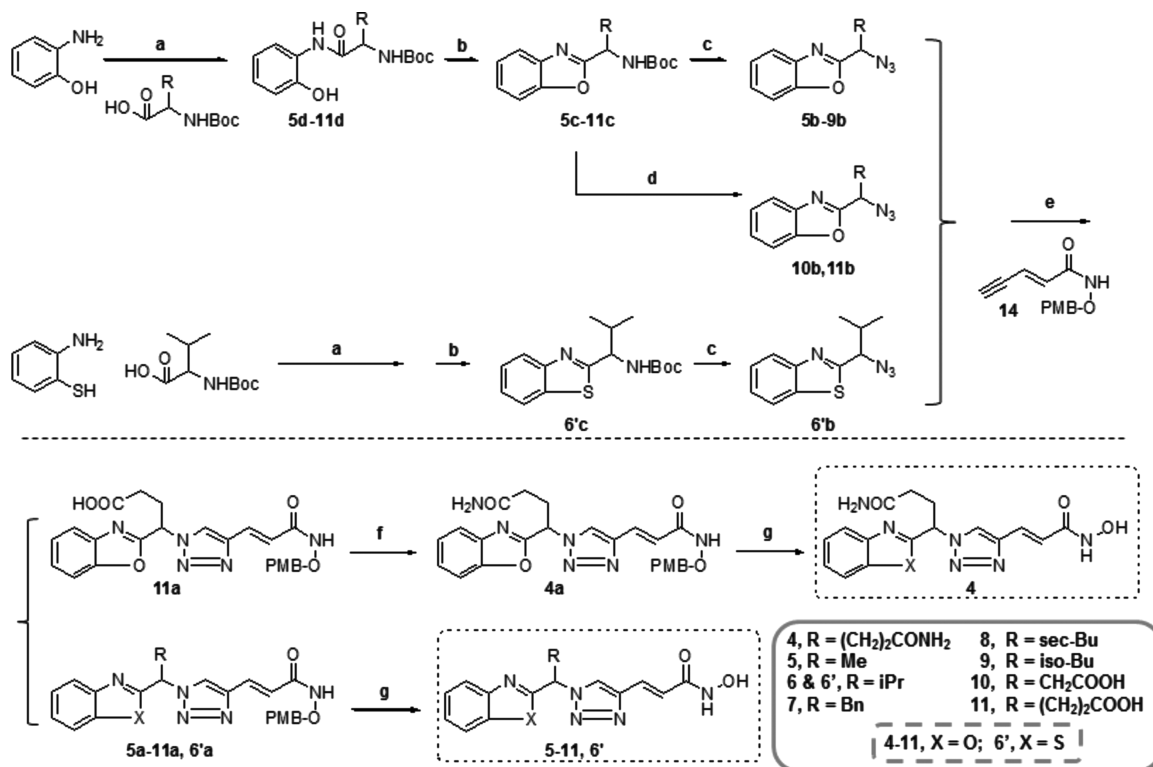


Figure 3. DFT calculations of favorable conformations for compounds 2 and 3.

inhibition assay data. Compound 2 was therefore taken as the optimal parent lead to enter into stage 2 studies.

**Stage 2: Introduction of a Side Chain onto the Middle Methylene Carbon Atom.** Initially in this stage,  $\beta$ -substituted racemic amino acid derivatives were employed as the reactants to prepare racemic target compounds 4–11, which were the branched derivatives of compound benzoxazole 2. As shown in Scheme 3, amidation reaction of *N*-Boc protected amino acid reactants with 2-aminophenol, followed by the intramolecular Mitsunobu reactions, afforded intermediates 5c–11c. For 5c–9c, the *N*-Boc protecting group was removed by the treatment with TFA in DCM; for 10c and 11c, a harsher acidic condition using 4 M hydrochloric acid in dioxane was employed to simultaneously remove both the *N*-Boc group and the *O*-Boc group. After routine workup manipulations, the obtained amino-group containing intermediates were directly converted to the azido compounds 5b–11b via the Cu(II)-mediated diazo transfer reaction. Huisgen cycloaddition reactions of the known alkyne compound 14 were carried out with 5b–11b using the catalyst of CuI·(POEt)<sub>3</sub> to afford the click products 5a–11a. The intermediate 4a was prepared via the amidation reaction of 11a. Finally, the PMB protecting group was removed by TFA to provide the target compounds 4–11. *In vitro* efficacy (Table 2) showed that target compounds in this stage with a middle-size and hydrophobic substitution group (6, *i*Pr; 8, *sec*-Bu; 9, *iso*-Bu) showed dramatically improved potency. Large substitution (7: Bn) or a negatively charged substitution (e.g., 10 or 11 with a carboxylic acid group) led to the decrease in potency. The target compound with a small substituent (5: Me) slightly enhanced the potency. For compound 4, which had a primary amide substituent, it was more potent than parent compound 2 in the HDAC inhibition assay, whereas the opposite trend was observed in MTT tests. Such inconsistency might originate from its poor permeability due to the high polar surface area of compound 4. To further explore the SAR, the benzothiazole derivative 6', which was the counterpart of benzoxazole derivative 6, was prepared. The synthesis of 6' followed exactly the same synthetic procedure of 6 (Scheme 3) using 2-aminothiopenol as the starting material, except that the initial amidation reaction product, after routine workup and without column purification, was directly employed in the next

Scheme 3. Syntheses of Recemic Target Compounds in Stage 2: 4–11 and 6<sup>a</sup>

<sup>a</sup>Reagents and conditions: (a) EDC, HOBT, DCM; (b) DIAD, PPh<sub>3</sub>, TEA; (c) (i) TFA, DCM, (ii) TfN<sub>3</sub>, NaHCO<sub>3</sub>, CuSO<sub>4</sub>; (d) (i) 4 M HCl in dioxane, (ii) TfN<sub>3</sub>, NaHCO<sub>3</sub>, CuSO<sub>4</sub>; (e) CuI·(POEt)<sub>3</sub>, DIPEA, THF, rt; (f) *N*-methyl piperidine, isobutyl chloroformate, NH<sub>3</sub>, -30 °C to -20 °C; (g) TFA, triisopropylsilane, DCM, rt.

Table 2. In Vitro Efficacy Assays of Compounds in Stage 2<sup>a</sup>

compds	IC <sub>50</sub> (nM) <sup>a</sup>		GI <sub>50</sub> (μM) <sup>b</sup>	
	HDACs	A549	HepG2	MDA-MB-231
SAHA	67	3.1	3.5	1.0
2	105	4.7	6.1	1.4
4	49	21.8	14.0	9.5
5	86	2.4	2.9	1.2
6	23	0.4	1.0	0.17
6'	5	1.9	1.9	0.93
7	219	4.4	5.9	5.5
8	4	0.52	1.7	0.19
9	19	0.66	2.2	0.28
10	140	>20	>20	>20
11	333	>20	>20	>20

<sup>a</sup>Mean of three independent triplicate experiments. <sup>b</sup>MTT data from our lab.

Mitsunobu reaction. Similar to the trend for compounds 1 and 2, the benzothiazole derivative 6' was more potent in the enzyme inhibition assay and less potent in MTT tests than benzoxazole derivative 6. It presumably was due to the metabolism viability of the sulfur-containing scaffold. To verify the hypothesis, we assessed the differential effects of the four compounds on the status of histone acetylation in MDA-MB-231 breast cancer cells. As shown in Figure 4, Western blot analysis showed that 5.0 μM compounds 1 and 6' induced significantly less acetylation of histone H3 compared to that of 5.0 μM compounds 2 and 6, respectively. Compound 6 was therefore taken as the optimal parent lead to enter into stage 3 studies.

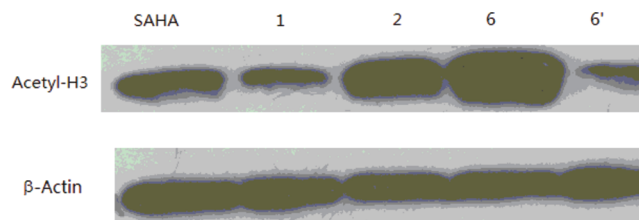
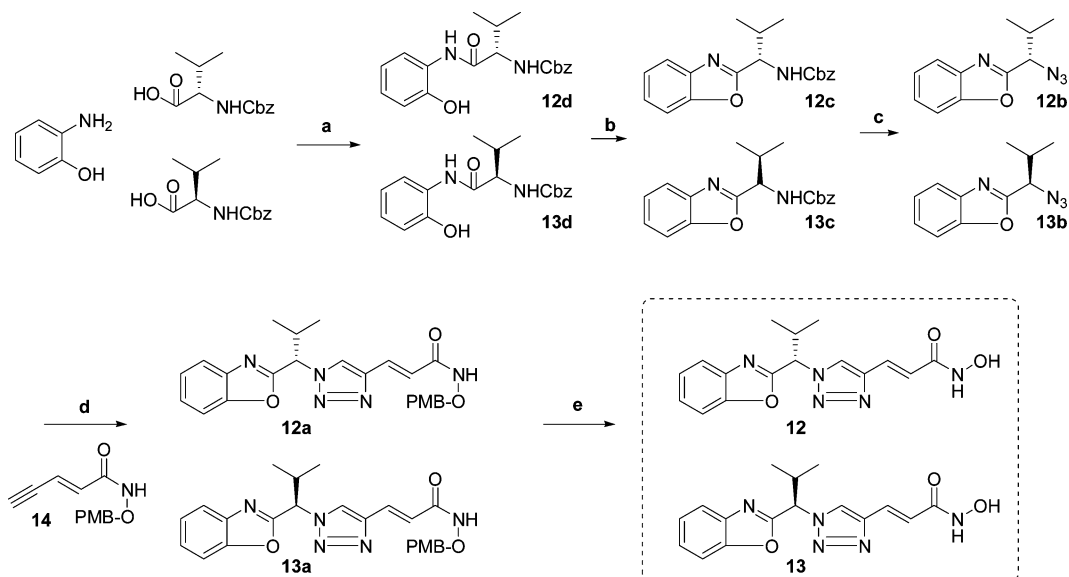


Figure 4. Effects of SAHA, compounds 1, 2, 6, and 6' on histone H3 acetylation expression at 5 μM after 24 h.

### Stage 3: Optically Pure Enantiomers of Compound 6.

The *S*-enantiomer 12 and the *R*-enantiomer 13 were prepared and evaluated in this stage. As shown in Scheme 4, the synthetic procedures of these two enantiomers were exactly the same as that of the racemic compound 6, except that the *N*-Boc protecting group was replaced with the *N*-Cbz protecting group, which could be removed in neutral conditions to avoid the racemization risks. Four pairs of enantiomers, including 12c and 13c, 12b and 13b, 12a and 13a, and 12 and 13 were all well characterized by chiral chromatography. The *S*-enantiomer 12 (IC<sub>50</sub> = 7 nM) was more potent than *R*-enantiomer 13 (IC<sub>50</sub> = 31 nM) in HDAC inhibition assays. Additionally, the inhibition capacities of compound 12 and SAHA against HDACs in living cells were compared. After the incubation with compound 12 or SAHA, AcH3 levels in MDA-MB-231 breast cancer cells were tested by Western blot analysis. As shown in Figure 5A, compound 12 and SAHA dose-dependently increased the acetylation of histone H3 after the cells were treated for 24 h. However, 5.0 μM compound 12 more significantly elevated the acetylation of histone H3

Scheme 4. Syntheses of Chiral Target Compounds in Stage 3: 12 and 13<sup>a</sup>

<sup>a</sup>Reagents and conditions: (a) EDC, HOBT, DCM; (b) DIAD, PPh<sub>3</sub>, TEA; (c) (i) Pd/C, H<sub>2</sub>, (ii) TfN<sub>3</sub>, NaHCO<sub>3</sub>, CuSO<sub>4</sub>; (d) CuI-(POEt)<sub>3</sub>, DIPEA, THF, rt; (e) TFA, triisopropylsilane, DCM, rt.

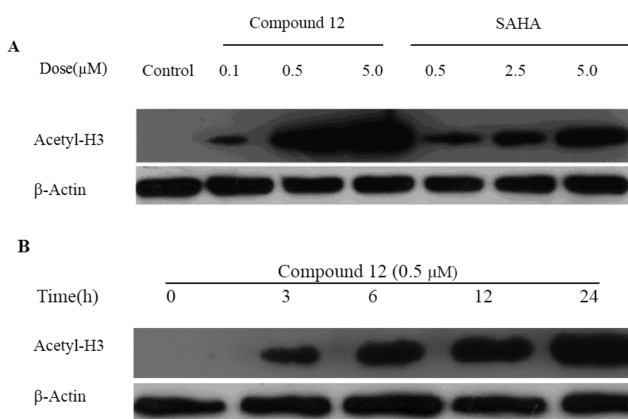


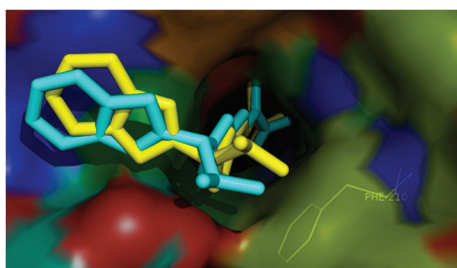
**Figure 5.** (A) Dose-dependent effect of compound 12 and SAHA on histone H3 acetylation. (B) Time-dependent effect of compound 12 on histone H3 acetylation at the concentration of 0.5  $\mu\text{M}$ .

compared to that of 5.0  $\mu\text{M}$  SAHA. Even 0.1  $\mu\text{M}$  compound 12 can dramatically induce the acetylation of histone H3. The acetylation of histone H3 after compound 12 treatment at 0.5  $\mu\text{M}$  for 3 h was detected and it increased in a time-dependent manner for 24 h (Figure 5B).

Both 12 and 13 were docked into the active site of the reported human HDAC2 crystal structure<sup>21</sup> (Figure 6). For

each isomer, two hydrophobic interactions with the rim region of HDAC2 protein were observed: (1) the benzoxazole ring with a shallow groove on the surface and (2) the isopropyl group with the Phe210 residue. For both of these two hydrophobic interactions, docking structures indicated that *S*-isomer 12 had a tighter interaction than *R*-isomer 13.

When a ligand molecule forms a complex with a protein, the molecular mobility is restricted to cause a loss of binding affinity due to the entropic penalty. Such a loss will be minimized if (1) the ligand's mobility is restricted by some intrinsic structural features; and (2) the dominant conformation of the ligand itself is close to its preferred conformation in the complex structure. Under such a guideline, our DFT calculations of single bond rotation barrier energies revealed an entropic contribution of the isopropyl substituent. The rotation energy barrier of the single bond of compound 12 was 3.9 kcal/mol higher than that of compound 2 (Figure 7). Additionally, as for the preferred conformations of compound 12 in the docking complex and by itself in gas phase, the C<sub>iPr</sub>-C<sub>chiral</sub>-N<sub>triazole</sub>-C<sub>triazole</sub> dihedral angles were 300° and 270°, respectively. In another word, the calculated low energy conformation of compound 12 by itself happened to be close to its dominant conformation in the docking structure, and the binding affinity was therefore enhanced. Compound 12 was named as NK-HDAC-1 to enter into the next stage.



HDAC inhibition (IC <sub>50</sub> )	
2 (without iPr substituent)	105 nM
<i>S</i> -enantiomer 12	7 nM
<i>R</i> -enantiomer 13	31 nM

**Figure 6.** Docking of 12 (in yellow) and 13 (in cyan) into the active pocket of human HDAC2.

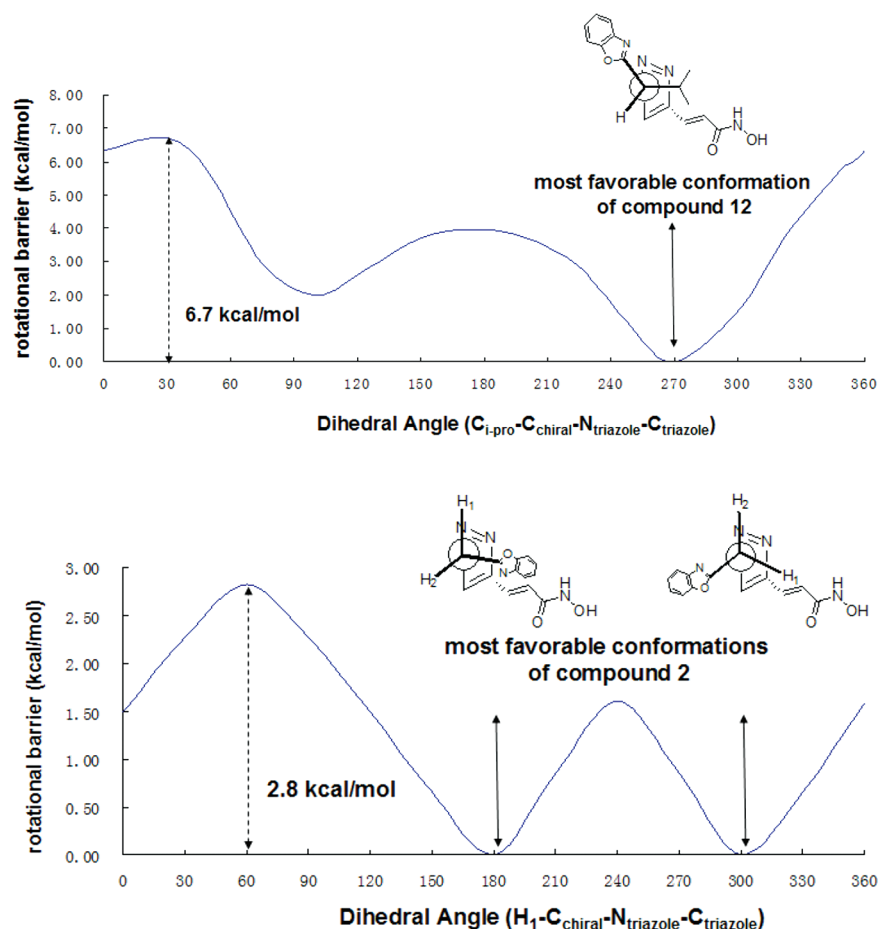


**Figure 7.** Relaxed coordinate scan using the QM method DFT (b3lyp) with the QM basic set 6-31G\*\*. The software is Jaguar, version 7.8 (Schrodinger, Inc., New York, NY, 2010). Dihedral angle ( $H_1-C_{chiral}-N_{triazole}-C_{triazole}$  or  $C_{i-pro}-C_{chiral}-N_{triazole}-C_{triazole}$ ) from  $0^\circ$  to  $360^\circ$ , increment  $5^\circ$ , total 73 point.

**Stage 4: Extensive *in Vitro* Assays to Evaluate the Potential of NK-HDAC-1 as a New Drug Candidate.** After the completion of HDAC inhibition assays, NK-HDAC-1 and its enantiomer 13 were both submitted to the National Cancer Institute (NCI) for acceptance into the human cancer cell line screening program (Table 3). For the 60 cell lines, the  $GI_{50}$  values of NK-HDAC1 mainly ranged between 100 to 500 nM. In detail, the  $GI_{50}$  values against leukemia cell lines ranged from 0.072 to 0.19  $\mu M$ ; the  $GI_{50}$  values against nonsmall cell lung tumor cell lines ranged from 0.010 to 0.54  $\mu M$ ; the  $GI_{50}$  values against colon cancer cell lines ranged from 0.038 to 0.47  $\mu M$ ; the  $GI_{50}$  values against CNS cancer cell lines ranged from 0.12 to 0.44  $\mu M$ ; the  $GI_{50}$  values against melanoma cell lines ranged from 0.044 to 0.22  $\mu M$ ; the  $GI_{50}$  values against ovarian cancer cell lines ranged from 0.027 to 0.70  $\mu M$ ; the  $GI_{50}$  values against renal cancer cell lines ranged from 0.044 to 0.362  $\mu M$ ; the  $GI_{50}$  values against prostate cancer cell lines ranged from 0.12 to 0.16  $\mu M$ ; and the  $GI_{50}$  values against breast cancer cell lines ranged from 0.051 to 0.52  $\mu M$ . In general, compound 12 was approximately 5-fold more potent than the *R*-enantiomer 13 and approximately 1 order of magnitude more potent than SAHA. Similar to SAHA, no significant specificities were observed among the tumor cells from different tissues. Besides the  $GI_{50}$  data of tumor cell lines from NCI, the  $GI_{50}$  values of NK-HDAC-1 and SAHA against nontransformed human breast cells MCF-10A were determined in our lab.  $GI_{50}$  values of NK-HDAC-1 against tumor breast cells were approximately 3 to 30

times lower than that of nontransformed breast cancer cells. Correspondingly, the difference for SAHA was 2 to 20 times. In summary, cell viability assay data indicated that NK-HDAC-1 should be more potent while having fewer *in vivo* side effects than SAHA.

Extensive *in vitro* pharmacokinetic (PK) related properties of NK-HDAC-1 were determined (Table 4). Its molecular weight is 327.1; its solubility in pH 7.4 PBS buffer is 20  $\mu g/mL$ ; and its  $LogD_{7.4}$  value is 2.0. All these physico-chemical properties are well acceptable for an oral drug candidate. The half-lives of NK-HDAC-1 in artificial gastric fluid, artificial intestinal fluid, mouse microsome, and mouse plasma are 9.4 h, > 24 h, 32 h, and 195 min respectively; comparatively, the corresponding data for SAHA are 22 h, > 24 h, 3.3 h, and 82 min. The apparent permeability ( $P_{app A \text{ to } B}$ ) of NK-HDAC-1 at 10  $\mu M$  is  $6.61 \times 10^{-6}$  cm/s, which is nearly four times higher than that reported for SAHA ( $1.70 \times 10^{-6}$ ).<sup>22</sup> Additionally, the efflux ratio of NK-HDAC-1 in Caco-2 permeability experiments is 1.15, indicating that NK-HDAC-1 should not be a substrate for P glycoprotein transporters. Since coadministration with other antitumor drugs is currently a main clinical research area for HDACi drug candidates, inhibition assays of human CYP enzyme by NK-HDAC-1 were performed. The  $IC_{50}$  values of NK-HDAC-1 and SAHA against human CYP3A4, a major CYP isozyme involved in the metabolism of approximately half of the marketed drugs, were 31.9  $\mu M$  and 24.8  $\mu M$  respectively, indicating that the possible drug–drug interaction side effects

Table 3. GI<sub>50</sub> Values of NK-HDAC-1 (Compound 12) in MTS and MTT Tests ( $\mu\text{M}$ )<sup>a,b</sup>

	12	13	SAHA		12	13	SAHA
	Leukemia				CNS Cancer		
CCRF-CEM	0.11	0.35	0.80	SF-268	0.33	0.63	1.6
HL-60(TB)	0.19	0.28	1.3	SF-295	0.12	0.31	1.6
K-562	0.088	0.28	0.50	SF-539	0.24	0.75	2.0
MOLT-4	0.072	0.30	0.40	SNB-19	0.43	0.85	0.63
SR	0.090	0.35	0.40	SNB-75	0.25	0.41	0.79
				U251	0.18	0.34	1.6
	Non-Small Cell Lung Cancer				Melanoma		
A549/ATCC	0.16	0.30	1.6	LOX IMVI	0.044	0.16	1.0
EKVX	0.24	0.68	1.3	MALME-3M	0.016	0.063	0.32
HOP-92	0.010	0.070	4.0	M14	0.18	0.41	1.3
NCI-H226	0.54	1.3	4.0	MDA-MB-435	0.091	0.24	0.50
NCI-H23	0.14	0.35	1.0	SK-MEL-2	0.087	0.35	1.3
NCI-H322M	0.14	0.25	0.79	SK-MEL-28	0.22	0.52	1.0
NCI-H460	0.15	0.39	0.79	SK-MEL-5	0.10	0.25	0.63
NCI-H522	0.013	0.13	0.50	UACC-257	0.088	0.23	0.50
				UACC-62	0.14	0.40	0.40
	Colon Cancer				Renal Cancer		
COLO 205	0.14	0.25	0.79	786-0	0.17	0.34	3.2
HCT-116	0.038	0.18	0.40	A498	0.18	0.26	1.6
HCT-15	0.47	0.96	2.5	ACHN	0.21	0.47	1.3
HT29	0.079	0.22	0.79	RXF 393	0.18	0.35	1.3
KM12	0.23	0.41	2.0	SN 12C	0.36	0.79	2.0
SW-620	0.13	0.29	0.63	TK-10	0.044	0.16	0.63
				UO-31	0.060	0.23	0.50
	Ovarian Cancer				Nontransformed Human Breast Cell Line		
IGROV1	0.056	0.19	1.3	MCF-10A <sup>c</sup>	1.6 <sup>c</sup>	ND <sup>d</sup>	9.6 <sup>c</sup>
OVCAR-3	0.22	0.47	1.3		Breast Cancer		
OVCAR-4	0.70	2.8	4.0	MDA-MB-468	0.15	0.25	0.63
OVCAR-5	0.14	0.40	0.79	HS 578T	0.58	1.3	5.0
OVCAR-8	0.084	0.24	0.50	BT-549	0.052	0.28	1.3
NCI/ADR-RES	0.027	0.095	0.16	T-47D	0.051	0.18	0.50
SK-OV-3	0.14	0.26	1.0	MDA-MB-231	0.52	0.91	2.5
				MCF7	0.18	0.45	2.0
	Prostate Cancer						
PC-3	0.12	0.28	2.0				
DU-145	0.16	0.35	1.3				

<sup>a</sup>Mean of three independent triplicate experiments. <sup>b</sup>All MTS data from NCI. <sup>c</sup>MTT data from our lab. <sup>d</sup>ND = not determined.

due to CYP3A4 inhibition by NK-HDAC-1 should be negligible.

## CONCLUSIONS

Conformationally constrained HDAC inhibitors bearing benzoxazole or benzothiazole cap moieties were synthesized via click chemistry. A promising chiral lead compound, NK-HDAC-1, with an isopropyl substituent showed approximately 10-fold greater potency than SAHA *in vitro*. The SAR data of efficacy were well rationalized by computational studies. Besides the hydrophobic interactions between NK-HDAC-1 and HDAC2 protein, this article specially addressed the significance of the rotation barrier of a single bond to the binding affinity, which would provide inspiring clues for future drug design programs. Additionally, the molecular weight of NK-HDAC-1 is only 327.1, which is lower than most of the HDACi drugs and candidates in clinical trials. It leaves great space for future lead optimization. Poor PK properties, including short *in vivo* half-life and low bioavailability, were the major problems for most of hydroxamate-containing HDACi in clinical trials. The *in vitro* PK data in this article

provided strong evidence that the *in vivo* PK properties of NK-HDAC-1 might be greatly superior to those of SAHA. In fact, our preliminary *in vivo* PK experiments using Balb/c mice showed that the bioavailability of NK-HDAC-1 was greater than 80%.<sup>23</sup> To the best of our knowledge, both of these two data were the best in class. In summary, our current data provided strong evidence to warrant future *in vivo* preclinical studies for NK-HDAC-1.

## EXPERIMENTAL SECTION

**HDAC Enzymes Assay.** The compounds were screened using purified HeLa cell nuclear extracts. The HDAC enzyme assay was based on the homogeneous fluorescence release assay in which deacetylation of the substrate, Ac-Arg-Gly-Lys(Ac)-AMC, generates a fluorophore that can be detected by a fluorometer.

**Inhibition of Cell Growth *in Vitro*.** Cells were seeded in 96-well plates and treated for 72 h with six serial compound dilutions. Cell viability was measured using an MTT assay which was performed following the manufacturer's protocol. The GI<sub>50</sub> value was obtained using Calcsyn software (Biosoft, Cambridge, UK). The results were derived from three independent experiments performed in triplicate.

**Table 4. PK Related *in Vitro* Properties of SAHA and NK-HDAC-1<sup>a</sup>**

		SAHA	NK-HDAC-1
molecular weight		264.2	327.1
solubility in pH 7.4 PBS buffer		>170 $\mu\text{g}/\text{mL}$ <sup>b</sup>	20 $\mu\text{g}/\text{mL}$ <sup>c</sup>
LogD in pH 7.4 PBS buffer		1.0 <sup>c</sup>	2.0 <sup>c</sup>
<i>in vitro</i> stability ( $t_{1/2}$ )	artificial gastric fluid	22 h <sup>c</sup>	9.4 h <sup>c</sup>
	artificial intestinal fluid	>24 h <sup>c</sup>	>24 h <sup>c</sup>
	plasma (mouse)	3.3 h <sup>c</sup>	32 h <sup>c</sup>
	micrisome (mouse)	82 min <sup>c</sup>	195 min <sup>c</sup>
human CYP 3A4 inhibition	24.8 $\mu\text{M}$ <sup>c</sup>	31.9 $\mu\text{M}$ <sup>c</sup>	
Caco-2 permeability assay at 10 $\mu\text{M}$	$P_{\text{app B to A}}$	$1.70 \times 10^{-6}$ cm/s <sup>e</sup>	$7.61 \times 10^{-6}$ cm/s <sup>c</sup>
	$P_{\text{app A to B}}$	ND <sup>f</sup>	$6.61 \times 10^{-6}$ cm/s <sup>c</sup>
	efflux ratio <sup>d</sup>	ND <sup>f</sup>	1.15 <sup>c</sup>

<sup>a</sup>Mean of three independent triplicate experiments. <sup>b</sup>See ref 27, determined in neutral water. <sup>c</sup>Data from our lab. <sup>d</sup>Defined by the ratio of  $P_{\text{app B to A}}$  over  $P_{\text{app A to B}}$ ; <sup>e</sup>see ref 22; <sup>f</sup>ND = not determined;

**Histone H3 Acetylation Assay.** MDA-MB-231 cells plated in a 35-mm dish were treated with compound **12** or SAHA at different concentrations for 24 h before the cells were trypsinized and washed with PBS. The treated cells were then lysed with RIPA lysis buffer containing 50 mM Tris-HCl (pH 7.5), 150 mM NaCl, 2 mM EDTA, 2 mM EGTA, 1 mM dithiothreitol, 1% Nonidet P-40, 0.1% SDS, protease inhibitors (1 mM PMSF, 5 mg/mL aprotinin, 5 mg/mL leupeptin, and 5 mg/mL pepstatin), and phosphatase inhibitors (20 mM  $\beta$ -glycerophosphate, 50 mM NaF, and 1 mM Na<sub>3</sub>VO<sub>4</sub>) for 30 min at 4 °C, and the supernatant was obtained after centrifuged at 12,000g, 4 °C for 20 min. The protein concentration was quantified by a BCA protein assay reagent kit (Beyotime Institute of Biotechnology). Identical amounts of protein (60  $\mu\text{g}$ ) from each sample were applied for SDS-PAGE and then transferred to the polyvinylidene difluoride membrane (Millipore, USA). The acetylation level was detected by primary antibody Antiacetyl-Histone H3 (Millipore, USA) and HRP-linked goat antirabbit secondary antibody (Santa Cruz Biotechnology, USA). The membrane was developed using enhanced chemiluminescence Western blot detection reagents (Millipore, USA).

***In Vitro* ADME Studies.** Solubility and logD were measured using the published methods.<sup>24</sup> Microsomal stability studies, caco-2 permeability assay, and CYP3A4 inhibition were performed according to published methods by Centaurus Biopharma, Ltd.

**Molecular Docking.** AutoDock 4.2<sup>25</sup> was used for the docking calculations. The AutodockTools<sup>26</sup> package was employed to generate the docking input files and to analyze the docking results. The charge of Zn and charge of O\* in R-CONHO\*H was set to +2 and -1, respectively. The torsion angle of O-C-N-O\* is set to 32.8°. A grid box size of 18.75  $\times$  18.75  $\times$  18.75 Å<sup>3</sup> with a spacing of 0.375 Å was implemented and covered almost the entire HDAC2<sup>21</sup> protein surface. Lamarckian genetic algorithm runs were set at 200 runs, with a population size of 200, a quaternum step of 30.0°, and a torsion step of 30.0°. All other parameter values were default values.

**DFT Calculation.** The geometries of compounds **2** and **3** were optimized using the DFT (B3LYP) method with the 6-31G\*\* basis set. The relaxed coordinate scan of compounds **12** and **2** was performed using the DFT (B3LYP) method with the 6-31G\*\* basis set. The dihedral angle (H<sub>1</sub>-C<sub>chiral</sub>-N<sub>triazole</sub>-C<sub>triazole</sub> or C<sub>i-pro</sub>-C<sub>chiral</sub>-N<sub>triazole</sub>-C<sub>triazole</sub>) was increased from 0° to 360° with a step of 5°. All the DFT calculations were performed using Jaguar 7.8.<sup>20</sup>

**Chemistry.** All reagents were purchased from Alfa Aesar and used without further purification. Thin-layer chromatography (TLC) was carried out on silica GF254 plates (Qingdao). Column chromatog-

raphy was performed on silica gel (200–300 mesh normal phase from Qingdao, or 200–400 mesh reverse phase from MED). <sup>1</sup>H and <sup>13</sup>C NMR spectra were obtained on a Bruker Avance 300 or 400 spectrometer, using tetramethylsilane as an internal standard. High resolution mass spectra (HRMS) were obtained on a QFT-ESI mass spectrometer.

Compound purity was determined by HPLC analysis on a Shimadzu LD-20A system with an ODS-C18 column (4.6  $\times$  150 mm, 5  $\mu\text{m}$ ) 1.2 mL/min over 15 min by UV at 220 nm. Enantiomeric excess (ee) determinations were carried out by chiral HPLC on a Chiral AD-H column, eluting with hexane/isopropanol/MeOH (containing 0.1% TFA) = 40:40:20 and detecting by UV at 254 nm.

**General Procedure for the Preparation of Click HDACi 1–13 and 6'.** Triisopropylsilane (3 mmol, 0.6 mL, 3 equiv), PMB protected substrate (**1a–13a** and **6'a**, 1 mmol, 1.0 equiv), and TFA (2 mL) were added in sequence to a reaction vessel containing DCM (40 mL). The mixture was stirred at room temperature and monitored by TLC. Upon completion, the reaction mixture was diluted with acetonitrile (100 mL) and then neutralized with DOWEX Marathon WBA anion exchange resin (from Aldrich). The resin was washed with acetonitrile (50 mL  $\times$  2). The combined organic solution was evaporated to provide a solid, which was purified to afford the final product.

**(E)-3-(1-((Benzo[d]thiazol-2-yl)methyl)-1H-1,2,3-triazol-4-yl)-N-hydroxyacrylamide (1).** Compound **1** was synthesized from compound **1a** following the general procedure. The crude product was purified via C-18 reverse phase chromatography (water/acetonitrile from 6:1 to 2.5:1) to give the product as a light yellow solid in 65% yield. <sup>1</sup>H NMR (500 MHz, DMSO-*d*<sub>6</sub>)  $\delta$  10.82 (br, s, 1H), 9.05 (br, s, 1H), 8.54 (s, 1H), 8.09 (apparent d,  $J = 7.9$  Hz, 1H), 7.98 (apparent d,  $J = 8.1$  Hz, 1H), 7.50–7.53 (m, 1H), 7.40–7.46 (m, 2H), 6.63 (d,  $J = 15.8$  Hz, 1H), 6.18 (s, 2H); <sup>13</sup>C NMR (125 MHz, DMSO-*d*<sub>6</sub>)  $\delta$  165.1, 162.3, 152.2, 143.3, 134.8, 126.8, 126.5, 125.7, 125.6, 122.8, 122.5, 120.0, 50.7. HRMS (–ESI) calcd for C<sub>13</sub>H<sub>10</sub>N<sub>5</sub>O<sub>3</sub>S [M – H]<sup>–</sup> 300.0561; found, 300.0554. Anal. RP-HPLC  $t_{\text{R}} = 8.12$  min (acetonitrile/water (containing 0.1% TFA) = 25:75; purity = 100%).

**(E)-3-(1-((Benzo[d]oxazol-2-yl)methyl)-1H-1,2,3-triazol-4-yl)-N-hydroxyacrylamide (2).** Compound **2** was synthesized from compound **2a** following the general procedure. The crude product was purified via C-18 reverse phase chromatography (water/acetonitrile from 6:1 to 2.5:1) to give the product as white solid in 50% yield. <sup>1</sup>H NMR (500 MHz, DMF-*d*<sub>7</sub>)  $\delta$  10.99 (br, s, 1H), 9.38 (br, s, 1H), 8.70 (s, 1H), 7.74–7.77 (m, 2H), 7.57 (d,  $J = 15.7$  Hz, 1H), 7.42–7.49 (m, 2H), 6.85 (d,  $J = 15.7$  Hz, 1H), 6.23 (s, 2H); <sup>13</sup>C NMR (125 MHz, DMF-*d*<sub>7</sub>)  $\delta$  160.7, 151.0, 144.1, 140.9, 127.2, 126.0, 125.7, 125.0, 120.31, 120.17, 111.0, 46.9 (one peak less due to overlap with solvent DMF-*d*<sub>7</sub>). HRMS (–ESI) calcd for C<sub>13</sub>H<sub>10</sub>N<sub>5</sub>O<sub>3</sub>[M – H]<sup>–</sup> 284.0789; found, 284.0783. Anal. RP-HPLC  $t_{\text{R}} = 6.01$  min (acetonitrile/water (containing 0.1% TFA) = 25:75; purity = 100%).

**(E)-3-(1-((1H-Benzo[d]imidazol-2-yl)methyl)-1H-1,2,3-triazol-4-yl)-N-hydroxyacrylamide (3).** Compound **3** was synthesized from compound **3a** following the general procedure. The crude product was purified via C-18 reverse phase chromatography (water/acetonitrile from 7:1 to 4:1) to give the product as a white solid in 50% yield. <sup>1</sup>H NMR (500 MHz, DMSO-*d*<sub>6</sub> + CF<sub>3</sub>COOD)  $\delta$  8.52 (s, 1H), 7.76 (br, s, 2H), 7.51 (br, s, 2H), 7.48 (d,  $J = 16$  Hz, 1H), 6.67 (d,  $J = 15.7$  Hz, 1H), 6.25 (s, 2H) (two active protons less); <sup>13</sup>C NMR (125 MHz, DMSO-*d*<sub>6</sub> + CF<sub>3</sub>COOD)  $\delta$  162.8, 147.7, 143.9, 131.5, 127.3, 126.5, 120.5, 118.3, 116.3, 114.6, 114.4, 112.5, 45.2. HRMS (–ESI) calcd for C<sub>13</sub>H<sub>11</sub>N<sub>6</sub>O<sub>2</sub> [M – H]<sup>–</sup> 283.0949; found, 283.0945. Anal. RP-HPLC  $t_{\text{R}} = 9.82$  min (acetonitrile/water (containing 0.1% TFA) = 10:90; purity = 100%).

**4-(4-((E)-2-(Hydroxycarbonyl)vinyl)-1H-1,2,3-triazol-1-yl)-4-(benzo[d]oxazol-2-yl)butanamide (4).** To a stirred solution of compound **11a** (0.1 mmol, 47 mg, 1.0 equiv.) in dry THF (1 mL) at –30 °C was added *N*-methyl piperidine (12  $\mu\text{L}$ , 1.1 equiv.), followed by isobutyl chloroformate (15  $\mu\text{L}$ , 1.1 equiv.). The reaction mixture was allowed to warm to –20 °C over 30 min, and then gaseous ammonia was then bubbled through the reaction mixture for 15 min. After warming to rt over 1 h, the reaction mixture was diluted with water, and the organic layer was separated. The aqueous layer was

extracted with DCM, and the combined organic extracts were dried over  $\text{Na}_2\text{SO}_4$  and concentrated under reduced pressure to give the desired compound **4a** as a light yellow solid. The PMB group was removed following the general procedure to afford the crude product. The crude product was purified via C-18 reverse phase chromatography (water/acetonitrile from 7:1 to 4:1) to give the product as a white solid (32%, 2 steps).  $^1\text{H}$  NMR (400 MHz,  $\text{DMSO}-d_6$ )  $\delta$  10.87 (s, 1H), 9.11 (s, 1H), 8.67 (s, 1H), 7.80 (d,  $J = 7.2$  Hz, 1H), 7.74 (d,  $J = 7.5$  Hz, 1H), 7.40–7.47 (m, 3H), 7.34 (s, 1H), 6.88 (s, 1H), 6.65 (d,  $J = 15.7$  Hz, 1H), 6.37 (apparent t,  $J = 7.4$  Hz, 1H), 2.75–2.81 (m, 1H), 2.56–2.67 (m, 1H), 2.06–2.20 (m, 2H);  $^{13}\text{C}$  NMR (100 MHz,  $\text{DMSO}-d_6$ )  $\delta$  172.5, 162.1, 150.3, 143.4, 140.0, 126.0, 125.0, 124.5, 120.18, 120.12, 111.2, 57.4, 30.2, 27.8 (two peaks less due to overlap). HRMS(–ESI) calcd for  $\text{C}_{16}\text{H}_{15}\text{N}_6\text{O}_4$   $[\text{M} - \text{H}]^-$  356.1160; found, 356.1161. Anal. RP-HPLC  $t_{\text{R}} = 6.83$  min (acetonitrile/water (containing 0.1% TFA) = 20:75; purity = 98.5%).

**(E)-3-(1-(1-(Benzo[d]oxazol-2-yl)ethyl)-1H-1,2,3-triazol-4-yl)-N-hydroxyacrylamide (5)**. Compound **5** was synthesized from compound **5a** following the general procedure. The crude product was purified via C-18 reverse phase chromatography (water/acetonitrile from 5:1 to 3:1) to give the product as a white solid in 45% yield.  $^1\text{H}$  NMR (400 MHz,  $\text{DMSO}-d_6$ )  $\delta$  8.65 (s, 1H), 7.78–7.81 (m, 1H), 7.72–7.75 (m, 1H), 7.39–7.46 (m, 3H), 6.64 (d,  $J = 15.8$  Hz, 1H), 6.48 (q,  $J = 7.0$  Hz, 1H), 2.05 (d,  $J = 7.0$  Hz, 3H) (two active proton less);  $^{13}\text{C}$  NMR (100 MHz,  $\text{DMSO}-d_6$ )  $\delta$  163.0, 162.3, 150.3, 143.3, 140.1, 126.7, 125.9, 124.9, 124.2, 120.13, 120.05, 111.1, 53.6, 18.3. HRMS(–ESI) calcd for  $\text{C}_{14}\text{H}_{12}\text{N}_5\text{O}_3$   $[\text{M} - \text{H}]^-$  298.0946; found, 298.0948. Anal. RP-HPLC  $t_{\text{R}} = 4.89$  min (acetonitrile/water (containing 0.1% TFA) = 30:70; purity = 97.9%).

**(E)-3-(1-(1-(Benzo[d]oxazol-2-yl)-2-methylpropyl)-1H-1,2,3-triazol-4-yl)-N-hydroxyacrylamide (6)**. Compound **6** was synthesized from compound **6a** following the general procedure. The crude product was purified via C-18 reverse phase chromatography (water/acetonitrile from 5:1 to 3:1) to give the product as a white solid in 44% yield.  $^1\text{H}$  NMR (400 MHz,  $\text{DMSO}-d_6$ )  $\delta$ : 8.66 (s, 1H), 7.82 (d,  $J = 7.3$  Hz, 1H), 7.76 (d,  $J = 7.6$  Hz, 1H), 7.40–7.48 (m, 3H), 6.65 (d,  $J = 15.7$  Hz, 1H), 6.11 (d,  $J = 9.1$  Hz, 1H), 2.89–2.97 (m, 1H), 1.04 (d,  $J = 6.4$  Hz, 3H), 0.87 (d,  $J = 6.4$  Hz, 3H) (two active proton less).  $^{13}\text{C}$  NMR (100 MHz,  $\text{DMSO}-d_6$ )  $\delta$ : 162.2, 161.6, 150.0, 143.3, 140.0, 126.5, 126.1, 125.0, 124.6, 120.2, 111.2, 63.3, 31.4, 19.0, 18.3 (one peak less due to overlap). HRMS(–ESI) calcd for  $\text{C}_{16}\text{H}_{16}\text{N}_5\text{O}_3$   $[\text{M} - \text{H}]^-$  326.1259; found, 326.1266. Anal. RP-HPLC  $t_{\text{R}} = 4.88$  min (acetonitrile/water (containing 0.1% TFA) = 40:60; purity = 99.1%).

**(E)-3-(1-(1-(Benzo[d]thiazol-2-yl)-2-methylpropyl)-1H-1,2,3-triazol-4-yl)-N-hydroxyacrylamide (6')**. Compound **6'** was synthesized from compound **6'a** following the general procedure. The crude product was purified via C-18 reverse phase chromatography (water/acetonitrile from 5:1 to 2:1) to give the product as a white solid in 48% yield.  $^1\text{H}$  NMR (400 MHz,  $\text{DMSO}-d_6$ )  $\delta$  10.85 (s, 1H), 9.10 (s, 1H), 8.67 (s, 1H), 8.06–8.15 (m, 2H), 7.47–7.58 (m, 3H), 7.43 (d,  $J = 15.7$  Hz, 1H), 6.66 (d,  $J = 15.7$  Hz, 1H), 6.15 (d,  $J = 9.7$  Hz, 1H), 2.87–2.96 (m, 1H), 0.99 (d,  $J = 6.4$  Hz, 3H), 0.87 (d,  $J = 6.3$  Hz, 3H);  $^{13}\text{C}$  NMR (100 MHz,  $\text{DMSO}-d_6$ )  $\delta$  167.5, 162.3, 151.9, 143.1, 134.7, 126.7, 126.6, 124.7, 123.1, 122.5, 120.1, 67.5, 33.2, 19.2, 18.7. HRMS(–ESI) calcd for  $\text{C}_{16}\text{H}_{16}\text{N}_5\text{O}_2\text{S}$   $[\text{M} - \text{H}]^-$  342.1030; found, 342.1031. Anal. RP-HPLC  $t_{\text{R}} = 5.32$  min (acetonitrile/water (containing 0.1% TFA) = 40:60; purity = 96.1%).

**(E)-3-(1-(1-(Benzo[d]oxazol-2-yl)-2-phenylethyl)-1H-1,2,3-triazol-4-yl)-N-hydroxyacrylamide (7)**. Compound **7** was synthesized from compound **7a** following the general procedure. The crude product was purified via C-18 reverse phase chromatography (water/acetonitrile from 5:1 to 3:1) to give the product as a white solid in 61% yield.  $^1\text{H}$  NMR (500 MHz,  $\text{DMSO}-d_6$ )  $\delta$  1.80 (br, s, 1H), 9.04 (br, s, 1H), 8.59 (s, 1H), 7.80 (d,  $J = 7.5$  Hz, 1H), 7.73 (d,  $J = 7.8$  Hz, 1H), 7.39–7.45 (m, 2H), 7.34 (d,  $J = 15.7$  Hz, 1H), 7.21–7.22 (m, 4H), 7.16–7.19 (m, 1H), 6.63–6.66 (m, 1H), 6.58 (d,  $J = 15.7$  Hz, 1H), 3.93 (dd,  $J_1 = 5.5$  Hz,  $J_2 = 14.2$  Hz, 1H), 3.79 (dd,  $J_1 = 10.5$  Hz,  $J_2 = 13.8$  Hz, 1H);  $^{13}\text{C}$  NMR (125 MHz,  $\text{DMF}-d_7$ )  $\delta$  162.8, 162.5, 150.7, 143.6, 140.5, 136.0, 129.5, 128.9, 127.5, 127.2, 126.6, 125.5, 125.2, 120.7, 120.6, 111.7, 59.4, 38.1. HRMS(–ESI) calcd for  $\text{C}_{20}\text{H}_{16}\text{N}_5\text{O}_3$

$[\text{M} - \text{H}]^-$  374.1259; found, 374.1250. Anal. RP-HPLC  $t_{\text{R}} = 6.78$  min (acetonitrile/water (containing 0.1% TFA) = 40:60; purity = 94.0%).

**(E)-3-(1-(1-(Benzo[d]oxazol-2-yl)-2-methylbutyl)-1H-1,2,3-triazol-4-yl)-N-hydroxyacrylamide (8)**. Compound **8** was synthesized from compound **8a** following the general procedure. The crude product was purified via C-18 reverse phase chromatography (water/acetonitrile from 5:1 to 2.5:1) to give the product as white solid in 45% yield.  $^1\text{H}$  NMR (400 MHz,  $\text{DMSO}-d_6$ )  $\delta$  10.85 (br, s, 1H), 9.12 (br, s, 1H), 8.69 (s, 1H), 7.82 (d,  $J = 7.3$  Hz, 1H), 7.77 (d,  $J = 7.9$  Hz, 1H), 7.39–7.48 (m, 3H), 6.64 (d,  $J = 15.7$  Hz, 1H), 6.16 (d,  $J = 9.4$  Hz, 1H), 2.68–2.75 (m, 1H), 1.19–1.26 (m, 1H), 1.06–1.13 (m, 1H), 0.99 (d,  $J = 6.7$  Hz, 3H), 0.86 (t,  $J = 7.3$  Hz, 3H);  $^{13}\text{C}$  NMR (100 MHz,  $\text{DMSO}-d_6$ )  $\delta$  162.2, 161.6, 150.0, 143.3, 139.9, 126.6, 126.1, 125.1, 124.7, 120.2, 120.1, 111.2, 62.3, 37.4, 24.4, 15.3, 10.5. HRMS(+ESI) calcd for  $\text{C}_{17}\text{H}_{20}\text{N}_5\text{O}_3$   $[\text{M} + \text{H}]^+$  347.1561; found, 347.1566. Anal. RP-HPLC  $t_{\text{R}} = 9.00$  min (acetonitrile/water (containing 0.1% TFA) = 35:65; purity = 99.4%).

**(E)-3-(1-(1-(Benzo[d]oxazol-2-yl)-3-methylbutyl)-1H-1,2,3-triazol-4-yl)-N-hydroxyacrylamide (9)**. Compound **9** was synthesized from compound **9a** following the general procedure. The crude product was purified via C-18 reverse phase chromatography (water/acetonitrile from 5:1 to 2.5:1) to give the product as a white solid in 48% yield.  $^1\text{H}$  NMR (400 MHz,  $\text{DMSO}-d_6$ )  $\delta$  10.86 (br, s, 1H), 9.14 (br, s, 1H), 8.71 (s, 1H), 7.80 (d,  $J = 7.5$  Hz, 1H), 7.74 (d,  $J = 7.5$  Hz, 1H), 7.40–7.46 (m, 3H), 6.65 (d,  $J = 15.7$  Hz, 1H), 6.41 (dd,  $J_1 = 5.6$  Hz,  $J_2 = 9.8$  Hz, 1H), 2.33–2.40 (m, 1H), 2.42–2.46 (m, 1H), 1.31–1.37 (m, 1H), 0.98 (d,  $J = 6.5$  Hz, 3H), 0.92 (d,  $J = 6.5$  Hz, 3H);  $^{13}\text{C}$  NMR (100 MHz,  $\text{DMSO}-d_6$ )  $\delta$  162.5, 162.2, 150.2, 143.2, 139.9, 126.6, 125.9, 124.9, 124.4, 120.1, 111.1, 56.3, 40.3, 24.2, 22.3, 21.2. HRMS(+ESI) calcd for  $\text{C}_{17}\text{H}_{20}\text{N}_5\text{O}_3$   $[\text{M} + \text{H}]^+$  342.1561; found, 342.1567. Anal. RP-HPLC  $t_{\text{R}} = 9.96$  min (acetonitrile/water (containing 0.1% TFA) = 35:65; purity = 99.3%).

**3-(4-((E)-2-(Hydroxycarbonyl)vinyl)-1H-1,2,3-triazol-1-yl)-3-(benzo[d]oxazol-2-yl)propanoic Acid (10)**. Compound **10** was synthesized from compound **10a** following the general procedure. The crude product was purified via C-18 reverse phase chromatography (water/acetonitrile from 7:1 to 4:1) to give the product as a white solid in 59% yield.  $^1\text{H}$  NMR (400 MHz,  $\text{DMSO}-d_6$ )  $\delta$  12.85 (br, s, 1H), 10.84 (s, 1H), 9.07 (s, 1H), 8.70 (s, 1H), 7.72–7.81 (m, 2H), 7.39–7.46 (m, 3H), 6.59–6.65 (m, 2H), 3.70 (dd,  $J_1 = 17.2$  Hz,  $J_2 = 6.7$  Hz, 1H), 3.56 (dd,  $J_1 = 17.2$  Hz,  $J_2 = 8.1$  Hz, 1H);  $^{13}\text{C}$  NMR (100 MHz,  $\text{DMSO}-d_6$ )  $\delta$  170.2, 162.2, 161.6, 150.2, 143.0, 139.8, 126.6, 126.0, 125.0, 124.9, 120.13, 120.06, 111.1, 54.2, 36.4. HRMS(–ESI) calcd for  $\text{C}_{15}\text{H}_{12}\text{N}_5\text{O}_5$   $[\text{M} - \text{H}]^-$  342.0844; found, 342.0852. Anal. RP-HPLC  $t_{\text{R}} = 5.88$  min (acetonitrile/water (containing 0.1% TFA) = 25:75; purity = 96.2%).

**4-(4-((E)-2-(Hydroxycarbonyl)vinyl)-1H-1,2,3-triazol-1-yl)-4-(benzo[d]oxazol-2-yl)butanoic Acid (11)**. Compound **11** was synthesized from compound **11a** following the general procedure. The crude product was purified via C-18 reverse phase chromatography (water/acetonitrile from 7:1 to 4:1) to give the product as a white solid in 55% yield.  $^1\text{H}$  NMR (400 MHz,  $\text{DMSO}-d_6$ )  $\delta$  10.85 (br, s, 1H), 9.10 (br, s, 1H), 8.68 (s, 1H), 7.82 (d,  $J = 6.9$  Hz, 1H), 7.74 (d,  $J = 8.2$  Hz, 1H), 7.40–7.47 (m, 2H), 6.65 (d,  $J = 15.7$  Hz, 1H), 6.40 (dd,  $J_1 = 6.1$  Hz,  $J_2 = 8.8$  Hz, 1H), 2.75–2.84 (m, 1H), 2.58–2.69 (m, 1H), 2.23–2.39 (m, 2H);  $^{13}\text{C}$  NMR (100 MHz,  $\text{DMSO}-d_6$ )  $\delta$  173.1, 162.3, 161.9, 150.3, 143.3, 140.0, 126.7, 126.0, 125.0, 124.6, 120.20, 120.16, 111.2, 57.1, 29.5, 27.5. HRMS(–ESI) calcd for  $\text{C}_{16}\text{H}_{14}\text{N}_5\text{O}_5$   $[\text{M} - \text{H}]^-$  356.1000; found, 356.1008. Anal. RP-HPLC  $t_{\text{R}} = 6.17$  min (acetonitrile/water (containing 0.1% TFA) = 25:75; purity = 95.3%).

**(E)-3-(1-((S)-1-(Benzo[d]oxazol-2-yl)-2-methylpropyl)-1H-1,2,3-triazol-4-yl)-N-hydroxyacrylamide (12)**. Compound **12** was synthesized from compound **12a** following the general procedure. The crude product was purified via C-18 reverse phase chromatography (water/acetonitrile from 5:1 to 3:1) to give the product as a white solid in 42% yield, ee = 91.3%.  $^1\text{H}$  NMR (400 MHz,  $\text{DMSO}-d_6$ )  $\delta$  10.80 (br, s, 1H), 9.10 (br, s, 1H), 8.66 (s, 1H), 7.82 (d,  $J = 7.9$  Hz, 1H), 7.76 (d,  $J = 7.4$  Hz), 7.39–7.48 (m, 3H), 6.65 (d,  $J = 15.7$  Hz), 6.11 (d,  $J = 9.2$  Hz, 1H), 2.88–2.97 (m, 1H), 1.03 (d,  $J = 6.6$  Hz, 3H), 0.86 (d,  $J = 6.6$  Hz, 3H);  $^{13}\text{C}$  NMR (100 MHz,  $\text{DMSO}-d_6$ )  $\delta$  162.3,

161.6, 150.1, 143.3, 139.9, 126.6, 126.1, 125.0, 124.7, 120.2, 120.1, 111.2, 63.4, 31.4, 19.0, 18.3. HRMS(–ESI) calcd for  $C_{16}H_{16}N_5O_3$  [ $M - H$ ]<sup>–</sup> 326.1259; found, 326.1265.

**(E)-3-(1-((R)-1-(Benzo[d]oxazol-2-yl)-2-methylpropyl)-1H-1,2,3-triazol-4-yl)-N-hydroxyacrylamide (13).** Compound 13 was synthesized from compound 13a following the general procedure. The crude product was purified via C-18 reverse phase chromatography (water/acetonitrile from 5:1 to 3:1) to give the product as white solid in 44% yield, ee = 92.1%. <sup>1</sup>H NMR (400 MHz, DMSO-*d*<sub>6</sub>) δ 10.83 (br, s, 1H), 9.09 (br, s, 1H), 8.67 (s, 1H), 7.83 (d, *J* = 7.2 Hz, 1H), 7.76 (d, *J* = 7.3 Hz, 1H), 7.40–7.48 (m, 3H), 6.65 (d, *J* = 15.8 Hz, 1H), 6.11 (d, *J* = 9.2 Hz, 1H), 2.88–2.97 (m, 1H), 1.03 (d, *J* = 6.7 Hz, 3H), 0.86 (d, *J* = 6.6 Hz, 3H); <sup>13</sup>C NMR (100 MHz, DMSO-*d*<sub>6</sub>) δ 162.3, 161.6, 150.1, 143.2, 139.9, 126.7, 126.1, 125.0, 124.7, 120.2, 120.1, 111.2, 63.3, 31.4, 19.0, 18.3. HRMS(–ESI) calcd for  $C_{16}H_{16}N_5O_3$  [ $M - H$ ]<sup>–</sup> 326.1259; found, 326.1266.

## ■ ASSOCIATED CONTENT

### 📄 Supporting Information

Full experimental details, NMR spectra, and chiral HPLC. This material is available free of charge via the Internet at <http://pubs.acs.org>.

## ■ AUTHOR INFORMATION

### Corresponding Author

\*Phone: (86) 022-23500781. Fax: (86) 022-23505369. E-mail: [pwang@nankai.edu.cn](mailto:pwang@nankai.edu.cn).

### Author Contributions

<sup>†</sup>These authors contributed equally to this work.

### Notes

The authors declare no competing financial interest.

## ■ ACKNOWLEDGMENTS

This study was supported by the National 973 Basic Research Program of China (No. 2010CB529100) and National Natural Science Foundation of China (No. 21072105). The HDAC inhibition assay was assisted by Dr. Wenfang Xu from Institute of Medicinal Chemistry School of Pharmaceutical Sciences, Shandong University. The cancer cell line MTS studies were performed by the NIH with the assistance from Dr. Robert Woodward.

## ■ REFERENCES

- (1) Shen, J.; Woodward, R.; Kedenburg, J. P.; Liu, X. W.; Chen, M.; Fang, L. Y.; Sun, D. X.; Wang, P. G. *J. Med. Chem.* **2008**, *51*, 7417–7427.
- (2) Kouzarides, T. Chromatin modifications and their function. *Cell* **2007**, *128*, 693–705.
- (3) Bernstein, B. E.; Meissner, A.; Lander, E. S. The mammalian epigenome. *Cell* **2007**, *128*, 669–681.
- (4) Li, E. Chromatin modification and epigenetic reprogramming in mammalian development. *Nat. Rev. Genet.* **2002**, *3*, 662–673.
- (5) Trojer, P.; Reinberg, D. Histone lysine demethylases and their impact on epigenetics. *Cell* **2006**, *125*, 213–217.
- (6) Yang, X. J.; Seto, E. The Rpd3/Hda1 family of lysine deacetylases: from bacteria and yeast to mice and men. *Nat. Rev. Mol. Cell Biol.* **2008**, *9*, 206–218.
- (7) Wolffe, A. P. Histone deacetylase: a regulator of transcription. *Science* **1996**, *272*, 371–372.
- (8) Wu, J.; Grunstein, M. 25 years after the nucleosome model: chromatin modification. *Trends Biochem. Sci.* **2000**, *25*, 619–623.
- (9) Marks, P. A.; Dokmanovic, M. Histone deacetylase inhibitors: discovery and development as anticancer agents. *Expert Opin. Invest. Drugs* **2005**, *14*, 1497–1511.

(10) Minucci, S.; Pelicci, P. G. Histone deacetylase inhibitors and the promise of epigenetic (and more) treatments for cancer. *Nat. Rev. Cancer.* **2006**, *6*, 38–51.

(11) Finnin, M. S.; Donigian, J. R.; Cohen, A.; Richon, V. M.; Rifkind, R. A.; Marks, P. A.; Breslow, R.; Pavletich, N. P. Structures of a histone deacetylase homologue bound to the TSA and SAHA inhibitors. *Nature* **1999**, *401*, 188–193.

(12) Cho, Y. S.; Whitehead, L.; Chen, C. H.; Jiang, L.; Francotte, E.; Richert, P.; Wagner, T.; Traebert, M.; Lu, Q.; Cao, X.; Dumotier, B.; Fejzo, J.; Rajan, S.; Wang, P.; Yan-Neale, Y.; Shao, W.; Atadja, P.; Shultz, M. Conformational refinement of hydroxamate-based histone deacetylase inhibitors and exploration of 3-piperidin-3-ylindole analogues of dacinostat (LAQ824). *J. Med. Chem.* **2010**, *53*, 2952–2963.

(13) Lu, Q.; Wang, D.-S.; Chen, C.-S.; Hu, Y.-D.; Chen, C.-S. Structure-based optimization of phenylbutyrate-derived histone deacetylase inhibitors. *J. Med. Chem.* **2005**, *48*, 5530–5535.

(14) Hou, J.; Feng, C.; Li, Z.; Fang, Q.; Wang, H.; Gu, G.; Shi, Y.; Liu, P.; Xu, F.; Zheng, Y.; Shen, J.; Wang, P. Structure-based optimization of click-based histone deacetylase inhibitors. *Eur. J. Med. Chem.* **2011**, *46*, 3190–3200.

(15) Yoshida, M.; Hoshikawa, Y.; Koseki, K.; Mori, K.; Beppu, T.. Structural specificity for biological activity of trichostatin A, a specific inhibitor of mammalian cell cycle with potent differentiation-inducing activity in Friend leukemia cells. *J. Antibiot.* **1990**, *43* (9), 1101–6.

(16) (a) Jagr, M.; Mraz, J.; Linhart, I.; Stransky, V.; Pospisil, M. Synthesis and characterization of styrene oxide adducts with cysteine, histidine, and lysine in human globin. *Chem. Res. Toxicol.* **2007**, *20*, 1442–52. (b) Coon, M. J.; Vaz, A. D. N.; McGinnity, D. F. peng, H.M. Multiple activated oxygen species in P450 catalysis: contributions to specificity in drug metabolism. *Drug Metab. Dispos.* **1998**, *26*, 1190–1193.

(17) Tamás Kálai, J. J.; Erzsébet, O.; Kálmán, H. *Synth. Commun.* **2003**, *33*, 1433–1442.

(18) Jernigan, F. E.; Sieracki, N. A.; Taylor, M. T.; Jenkins, A. S.; Engel, S. E.; Rowe, B. W.; Jové, F. A.; Yap, G. P. A.; Papish, E. T.; Ferrence, G.M.. Sterically bulky tris(triazolyl)borate ligands as water-soluble analogues of tris(pyrazolyl)borate. *Inorg. Chem.* **2007**, *46*, 360–362.

(19) Bloom, A.; Day, A. R. The Preparation of 2-Alkylaminobenzimidazoles. *J. Org. Chem.* **1939**, *4*, 14–19.

(20) *Jaguar*, version 7.8; Schrodinger, LLC: New York, 2011.

(21) Cronin, C. N.; Hilgers, M. T.; Knuth, M. W.; Navre, M. E.; Sang, C.; Skene, R. J.; Tari, L. W.; Wilson, K. P.; Witemer, D.; Zou, H. Crystallization of Histone Deacetylase 2. US 7507552 B1, 2009; pp 197

(22) FDA approval and new drug application (NDA) documents for Zolinza (SAHA, vorinostat). [http://www.accessdata.fda.gov/drugsatfda\\_docs/nda/2006/021991s000\\_ZolinzaTOC.cfm](http://www.accessdata.fda.gov/drugsatfda_docs/nda/2006/021991s000_ZolinzaTOC.cfm)

(23) Guo, W.; Lu, Y.; Li, R.; Li, Y.; Li, Z.; Hou, J.; Liu, R.; Yuan, S.; Shen, J.; Wang, P. G. Preclinical evaluations of NK-HDAC-1 as a new anti-cancer drug candidate. The results will be published in the future

(24) Wang, H.; Lim, Z.-Y.; Zhou, Y.; Ng, M.; Lu, T.; Lee, K.; Sangthongpitag, K.; Goh, K. C.; Wang, X.; Wu, X.; Khng, H. H.; Goh, S. K.; Ong, W. C.; Bonday, Z.; Sun, E. T. Acylurea connected straight chain hydroxamates as novel histone deacetylase inhibitors: synthesis, SAR, and in vivo antitumor activity. *Bioorg. Med. Chem. Lett.* **2010**, *20*, 3314–3321.

(25) Morris, G. M.; Goodsell, D. S.; Halliday, R. S.; Huey, R.; Hart, W. E.; Bewle, R. K.; Olson, A. J. Automated docking using a Lamarckian genetic algorithm and empirical binding free energy function. *J. Comput. Chem.* **1998**, *19*, 1639–1662.

(26) Sanner, M. F. Python: A programming language for software integration and development. *J. Mol. Graphics Modell.* **1999**, *17*, 57–61.

(27) Cai, Y. Y.; Yap, C. W.; Wang, Z.; Ho, P. C.; Chan, S. Y.; Ng, K. Y.; Ge, Z. G.; Lin, H. S. Solubilization of vorinostat by cyclodextrins. *J. Clin. Pharm. Ther.* **2010**, *35* (5), 521–526.